

Model-Based Development of Leaping in a Hexapod Robot

Ya-Cheng Chou, Ke-Jung Huang, Wei-Shun Yu, and Pei-Chun Lin, *Member, IEEE*

Abstract—We report on the model-based development of leaping behavior in a RHex-style hexapod robot. A three-legged model is proposed to analyze the dynamic behavior of leaping, and this serves as a guide for implementing the behavior on the empirical robot. The model has a rigid body and three massless and compliant legs, which have rolling contact with the ground for better modeling the leg behavior of the empirical robot. By investigating the model's behavior, a two-step leaping maneuver is developed. The first step is utilized for adjusting the body pitch, synchronizing the phases of all six legs, and speeding up the body's forward velocity. This provides adequate initial conditions for the second step leaping, which creates a long-distance flight and adequate landing for follow-up running. In addition, we also report on the strategy of stride length regulation. With implementation of the range sensor, the robot can regulate its stride in order to reach a specific and desired position for leaping. The gait transition and initiation of leaping is fully autonomous. The behavioral development is implemented in the RHex-style robot and is evaluated experimentally.

Index Terms—Behavior development, gait transition, hexapod, leaping, three-leg model.

I. INTRODUCTION

LEAPING is one of the unique behaviors performed by legged animals, which allows the creature to rapidly change the status of its original motion. While walking/running usually serves as the nominal gait for locomotion, animals use leaping in life-dependent situations such as hunting prey or escaping from predators. They also use leaping to negotiate ex-

tremely challenging terrain and obstacles. On the scientific and engineering side, leaping is an interesting locomotion method because it has a unique characteristic: It is fast and dynamic, yet has minimum requirements on the terrain because it utilizes very few ground contact points per displacement during locomotion. Thus, as the terrain becomes rougher and more challenging, leaping is still more likely than other gaits to be functional. From this aspect, leaping can be regarded as the extreme scenario of running since the latter is also dynamic and requires few ground contact points during locomotion. Thus, understanding how to initiate leaping behavior as well as its transition from and to running would extend the region of dynamic running locomotion to a wider and deeper domain.

Because leaping/jumping by nature requires large power input and special body maneuvers, it is usually difficult to generate on legged robots that are originally designed for walking or running. Therefore, the approaches adopted by researchers involve either designing jumping-specialized robots or installing extra actuators and mechanisms for jumping on the original walking robots. Examples of the former include the miniature 7-g robot that can jump much higher than its height by a four-bar linkage with elastic elements and supply power [1], the MSU jumper that is steerable [2], and the flea-inspired jumping robot that is driven by shape memory alloy spring actuators [3]. The robot Grillo also accomplishes continuous jumping by storing elastic energy in a mechanism [4], [5]. The frog robot Mowgli can jump over 50% of its body height by pneumatic muscle actuators [6]. Examples of the latter are: the quadruped robot Mini-Whigs, which has a springy four-bar linkage installed in the body for jumping behavior [7], [8]; the wheeled robot SandFlea, which has a piston actuator with fuel cartridge, and can jump 8 m high [9]; the two-wheel cylindrical robot Scout, which has a spring foot for jumping [10], [11]; and a surveillance robot, which adds an extra six-bar linkage mechanism with a spring for hopping [12]. In addition to the legged robots, some spherical robots have jumping functionality to increase their mobility—for example, by a deformable shell or an internal mechanism [13], [14].

Only a few works relate to developing jumping-like behavior in ordinary walking or running robots. On the simulation side, a quadruped standing jump over an obstacle was performed, mimicking ordinary jumping behavior of a quadruped animal such as a horse [15], [16]. Bounding of a quadruped [17], [18] and pronking of a hexapod [19] have been simulated as well. On the robot side, various pneumatic-actuated legged robots with dynamic maneuvering have been reported [20]. A quadruped robot with hydraulic actuators can perform trotting, pacing, and bounding [21]. The leg-wheel hybrid quadruped AirHopper can produce enough power to lift itself to 57% of body height by its

Manuscript received August 5, 2014; accepted November 19, 2014. Date of publication December 18, 2014; date of current version February 4, 2015. This paper was recommended for publication by Associate Editor S. Kim and Editor A. Kheddar upon evaluation of the reviewers' comments. This work was supported by the National Science Council, Taiwan, under contract 100-2628-E-002-021-MY3. This paper was presented in part at the 2013 International Conference on Climbing and Walking Robots (partial results of Section II and III).

Y. C. Chou was with the Department of Mechanical Engineering, National Taiwan University, Taipei 10617, Taiwan. He is now with GARMIN Corporation, New Taipei City 221, Taiwan (e-mail: r99522805@ntu.edu.tw).

K. J. Huang was with the Department of Mechanical Engineering, National Taiwan University, Taipei 10617, Taiwan. He is now with Pegatron Corporation, Taipei 11261, Taiwan (e-mail: b95502111@ntu.edu.tw).

W. S. Yu was with the Department of Mechanical Engineering, National Taiwan University, Taipei 10617, Taiwan. He is now with Kinpo Electronics Inc., Taipei 10571, Taiwan (e-mail: randyko26@gmail.com).

P. C. Lin is with the Department of Mechanical Engineering, National Taiwan University, Taipei 10617, Taiwan (e-mail: peichunlin@ntu.edu.tw).

This paper has supplementary downloadable material available at <http://ieeexplore.ieee.org>, provided by the author. The material consists of two videos: one video shows the robot leaping over a ditch, Leap (ditch).mpg (size: 1.23 MB), and the other one shows the robot leaping over an obstacle, Leap(obstacle).mpg (size: 2.98 MB). Contact peichunlin@ntu.edu.tw for further questions about this work.

Color versions of one or more of the figures in this paper are available online at <http://ieeexplore.ieee.org>.

Digital Object Identifier 10.1109/TRO.2014.2376141

eight air cylinders [22]. Another leg-wheel hybrid quadruped, PAW, can jump a short step by matching front and hind leg motion [23]. The quadruped LittleDog can jump to pass an obstacle via an optimization method [24], [25]. The biped robot MARI-3 has been developed for vertical jumps [26]. The hexapod RHex [27] can jog [28] or pronk [29], [30]. A recent work on RHex shows that by finding an achievable state sequence formed by various possible body configurations, RHex can also perform ditch leaping and various other dynamic maneuvers because the transition between states naturally excites the dynamics of the robot [31]. One of the great advantages of this approach is that various dynamic behaviors can be found simultaneously if various feasible paths of state transitions are observed. However, and in the meantime, some tuning is still required to make the robot behavior repeatable and robust. The locomotion performed by these empirical robots is indeed fantastic, and the associated development moves the study of legged robotics to a multifunctional dynamic region. These developments also reveal that power density is the critical issue for the robots to initiate dynamics. The hydraulic and pneumatic systems have higher power density but burdened with complex power-autonomous setting up. The power-autonomous legged systems with electric motors often rely on passive springs to help excite the dynamic behaviors. Yet some limited work relating to leaping with large-distance flight has revealed that it is still very challenging to do so because of its highly dynamic characteristics, not to mention the transition between leaping and other gaits. To the best of our knowledge, BigDog is the only robot showing leaping behavior, which is transient from running. However, the demonstrations are only provided in movie clips with no detailed documentation [32].

Here, a model-based leaping behavior developed in a RHex-style robot is reported. In particular, the work focuses on developing the leaping transition from running [i.e., given running as the initial condition (I.C.) for leaping]. Thus, an animal-like leaping behavior (or hurdling) can be performed in an artificial legged platform. Although the RHex-style hexapod robot has only 1 degree of freedom (DOF) per leg, the combined trajectories versus time of all six legs have unlimited combinations, and it is extremely hard to empirically explore the leaping behavior by trial and error. Thus, a model-based approach is adopted. A reduced-order planar three-leg model is proposed, and by analyzing its dynamic behavior via systematic parameter and state variations, a feasible leaping behavior and its transition from running on the model can be formulated. At the same time, because of the existence of the dynamic model, the mechanism of leaping can also be revealed by Newtonian mechanics. This model development then served as a guide to initiate the same behaviors on the RHex-style robot shown in Fig. 1(a). Thus, the proposed model-based robot behavioral development is experimentally evaluated, and the performance and difference between the model and the empirical system can be addressed.

Section II introduces the design concept of the planar three-leg model and is followed by Section III, which describes the process of designing the leaping maneuver. Section IV reports the method of transiting the gait from running to leaping.

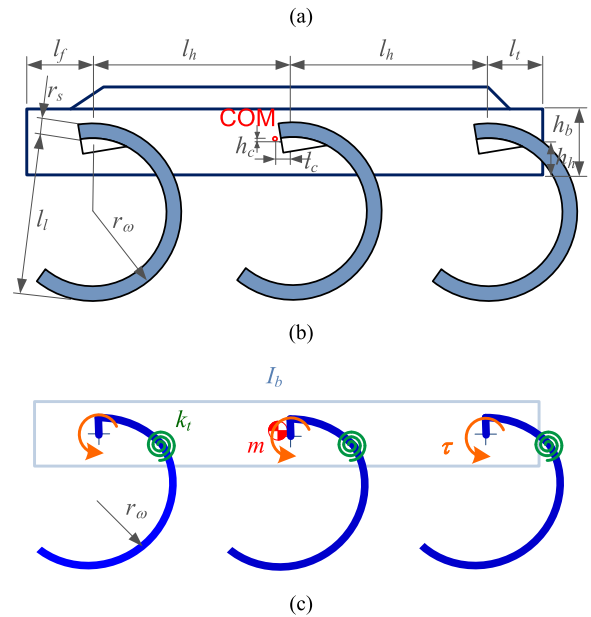
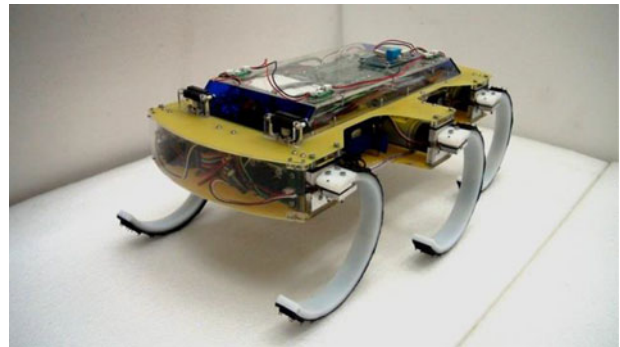


Fig. 1. Robot and model. (a) Photo of the RHex-style hexapod robot. (b) Robot dimension symbols for model development. (c) Sketch of the three-leg model.

Section V reports on the experimental evaluation of the robot and Section VI concludes this paper.

II. PLANAR MODEL WITH THREE COMPLIANT LEGS

The three-leg planar model shown in Fig. 1(c) is utilized for developing the leaping behavior. It consists of three massless legs and a rigid body with mass m at the center of mass (COM) and mass moment of inertia I_b . The circular leg has a torsion spring with stiffness k_t (i.e., a compliant leg) and is driven by torque input τ . When the leg contacts the ground and moves, it is assumed to exhibit pure rolling behavior. The morphology of the model is determined by various considerations, which are described as follows.

The multileg planar model is suitable for analyzing the dynamics of leaping behavior. In general, leaping by animals or robots mainly involves a dramatic motion change in the fore/aft and vertical directions of locomotion. A planar dynamic model in the sagittal plane is adequate for analyzing this specific type of motion. It preserves the essential portion of the spatial motion and ignores the rest, unless simultaneous leaping-and-turning

behavior is investigated. In addition, multileg morphology and torque input are adopted to provide the model with agile maneuverability. Although a spring-loaded inverted pendulum (SLIP) model [33]–[35] is widely used as the “template” [36] to represent running behavior of animals or robots, its one virtual leg morphology, as well as its energy-conservative nature, limits its dynamic maneuverability for rapid state change as required in leaping. Besides, the robot in general has a multileg morphology; therefore, if the SLIP model is utilized as the template for leaping behavior [36], it would require the development of mapping from multiple legs to one virtual leg and *vice versa*, which is complex. In contrast, the three-legged model preserves the six-legged structure of insects or hexapod robots by collapsing the right and left legs into one. The mapping between the model and the empirical robot is straightforward, and the model’s level of maneuverability is identical to the original system for leaping behavior.

The use of massless and compliant legs in the three-leg model follows the usual analysis setting for these template-style dynamic models. As with the SLIP model, the compliant leg helps to excite the dynamic behavior of the model, and its massless setting simplifies complexity of analysis in two aspects: one is to reduce DOFs of the model, and the other is to obviate the need for an impact model. In addition, several new template-style models have been recently reported, such as SLIP-R with linear spring and rolling foot [37], C-Pod with a large half-circle shape [38], and CT-SLIP [39] and SLIP-T [19] with motor torque and leg damping. Different modifications were added to these new models, but the assumption of using massless legs is common to all. Empirically, the setup of massless and compliant legs on the model is also reasonable for the RHex-style robot whose legs are made by lightweight polymers or composites [27], [40], [41]. The mass of all legs is less than 10% of the robot mass.

The morphology of the compliant legs in the three-leg model is determined by the leg characteristics of the RHex-style robot, which is utilized for experimental evaluation of the proposed work. The compliant half-circular leg of the RHex-style robot has two characteristics, which cannot be captured by an ordinary linear spring: rolling contact and varying compliance determined by the ground contact point of the leg at every instant. Thus, instead of using a linear spring as in the traditional SLIP model, a leg model with the above two characteristics is utilized in the proposed work, which is extracted from the “virtual leg” of our recently developed and template-style model called Rolling SLIP (R-SLIP) [42]. The leg has two segments connected by a torsion spring as shown in Fig. 2(b). The upper segment connects the leg to the body, and the lower segment has a circular shape, providing rolling contact to the ground. Because the length of moment arm changes as the leg rolls, the equivalent linear stiffness between the hip and ground-contact point varies accordingly. As a result, two characteristics of the half-circular leg on the RHex-style robot can be adequately captured by the legs of the proposed three-leg model; therefore, the model behavior can have less discrepancy with the empirical robot. Note that the methodology of the following development can also be deployed to robots with other types of legs such as linear springs. The use of a rolling leg in this study is mainly

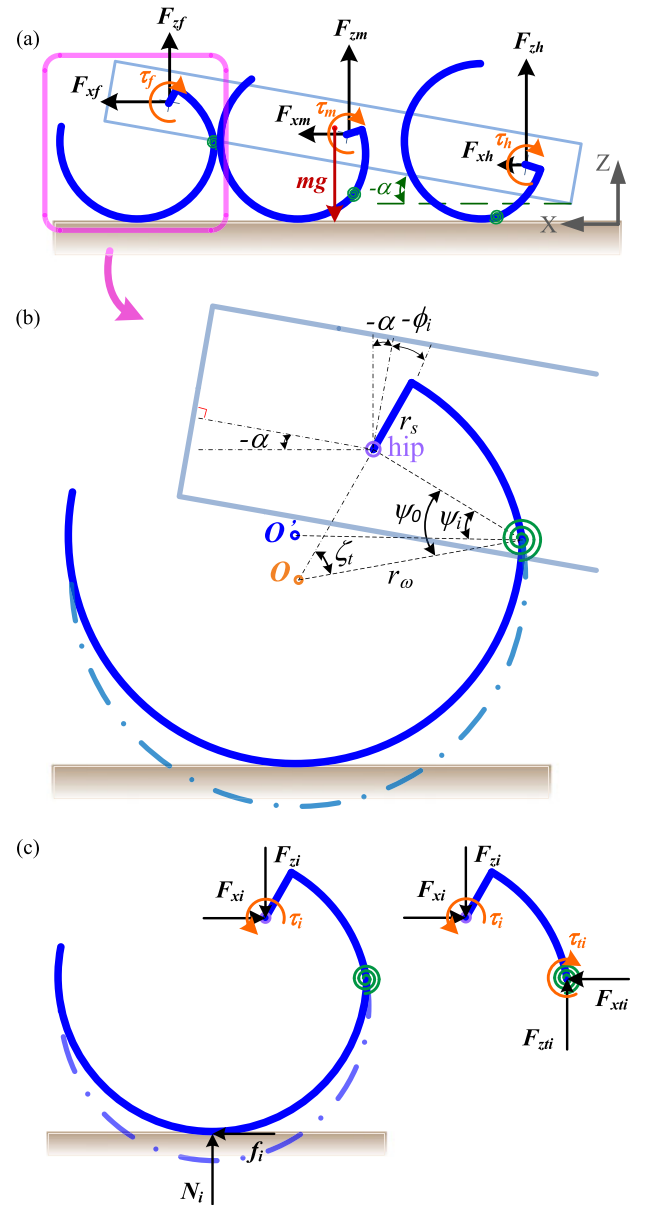


Fig. 2. Illustration of the dynamic models. (a) Three-leg model and its free body diagram of the body. (b) R-SLIP model for the compliant half-circular leg, where the robot body is sketched in a dashed line. The R-SLIP model is composed of two leg segments (blue solid line and arc) connected by torsion springs (green spiral). The leg in its neutral configuration is plotted in an orange dash-dotted arc. (c) Free body diagram of the leg.

for providing the conditions for validating the empirical robot in the lab. As a side note, the leg-wheel transformable robots Quattroped and TurboQuad also use legs with similar morphology [43], [44].

With the assumption of rolling contact, the planar three-leg model has only three DOFs. This characteristic can be addressed by analyzing the leg compression/uncompression behavior as shown in Fig. 2(b). The following leg parameters are used: O is the center of the circular leg in its natural configuration, r_w and r_s are leg geometrical parameters, ξ_t defines the location of the torsional spring on the leg, ψ_o represents the angle of the

spring in its natural configuration, α is body pitch angle, and ϕ_i is the orientation of the leg with respect to the robot body. The subscript i throughout the paper is the general index to identify the leg in use, where f , m , and h represent front, middle, and hind, respectively. In general, if the legs can slide on the ground, the model has six DOFs. In this case, even if we know the model's body configuration (i.e., COM displacement and body pitch), the leg configurations at every instant during motion still cannot be solved unless either the leg orientations (ϕ_f , ϕ_m , ϕ_h) or compressions (ψ_f , ψ_m , ψ_h) are given. In contrast, if the model legs have pure rolling contact on the ground, the six variables (ϕ_f , ϕ_m , ϕ_h , ψ_f , ψ_m , ψ_h) are related to each other by geometrical constraints. In this case, with a given 3-DOF body configuration and the initial leg configurations, the leg configurations throughout the compression/decompression motion can be derived. As a result, only three variables are required to represent the motion of the three-leg model. The classic choice for behavioral analysis is body state, including COM translation (X_c , Z_c) and body pitch (α). To ease numerical computation, another set of variables is chosen: hind leg orientation (ϕ_h), hind leg compression (ψ_h), and body pitch (α).

The quantitative derivation of the three-leg model in an inertial frame is described as follows. There are nine external forces/moments acting on the body as shown in Fig. 2(a). Each hip has one torque, τ_i , and two reaction forces in the fore/aft direction, F_{xi} , and vertical direction, F_{zi} . With these definitions, three equations of motion (EOM) can be formulated, including a force EOM in the horizontal direction

$$F_{xh} + F_{xm} + F_{xf} = m\ddot{X}_c \quad (1)$$

a force EOM in the vertical direction

$$F_{zh} + F_{zm} + F_{zf} - mg = m\ddot{Z}_c \quad (2)$$

and a moment EOM with respect to the model COM:

$$\begin{aligned} & \tau_h + \tau_m + \tau_f + F_{xh}((l_h + l_c) \sin(-\alpha) + h_c \cos(-\alpha)) \\ & + F_{xm}(l_c \sin(-\alpha) + h_c \cos(-\alpha)) \\ & + F_{xf}(-(l_h - l_c) \sin(-\alpha) + h_c \cos(-\alpha)) \\ & - F_{zh}((l_h + l_c) \cos(-\alpha) - h_c \sin(-\alpha)) \\ & + F_{zm}(l_c \cos(-\alpha) - h_c \sin(-\alpha)) \\ & + F_{zf}((l_h - l_c) \cos(-\alpha) + h_c \sin(-\alpha)) = I_b \ddot{\alpha} \end{aligned} \quad (3)$$

where l_h , l_c , and h_c are dimensions of the robot depicted in Fig. 1(b). The symbol I_b is the mass moment of inertia. Next, the COM acceleration, the forces, and the torques listed in (1)–(3) should be represented as functions of variables (ϕ_h , ψ_h , α); therefore, the EOM can be solved for further analysis.

Representing the COM accelerations (\ddot{X}_c , \ddot{Z}_c) as functions of variables (ϕ_h , ψ_h , α) can be achieved by formulating the state in two steps. First, formulate the COM accelerations as functions of the body pitch, its derivatives, and acceleration of the hind hip (\ddot{X}_{hh} , \ddot{Z}_{hh}). The COM acceleration in the horizontal direction is described as

$$\begin{aligned} \ddot{X}_c = & \ddot{X}_{hh} - (l_h + l_c) \cos(-\alpha)(\dot{\alpha})^2 - (l_h + l_c) \sin(-\alpha)(\ddot{\alpha}) \\ & + h_c \sin(-\alpha)(\dot{\alpha})^2 - h_c \cos(-\alpha)(\ddot{\alpha}) \end{aligned} \quad (4)$$

and the COM acceleration in the vertical direction is

$$\begin{aligned} \ddot{Z}_c = & \ddot{Z}_{hh} - (l_h + l_c) \sin(-\alpha)(\dot{\alpha})^2 + (l_h + l_c) \cos(-\alpha)(\ddot{\alpha}) \\ & - h_c \cos(-\alpha)(\dot{\alpha})^2 - h_c \sin(-\alpha)(\ddot{\alpha}). \end{aligned} \quad (5)$$

The equations shown in (4) and (5) are yielded from a double derivation of the geometrical relation between the COM and the hind hip. Second, displacements of the hips (X_{ih} , Z_{ih}) can further be linked to leg states. The displacement of the hip in the horizontal direction can be described as

$$\begin{aligned} X_{ih} = & X_{ic0} + r_\omega(\phi_i + \alpha - \phi_{i0} - \alpha_0 - \psi_0 + \psi_i) \\ & + r_\omega \sin(\phi_t - \phi_i - \alpha) - r_\omega \sin(\phi_t - \phi_i - \alpha) \\ & + \psi_0 - \psi_i + r_s \sin(\phi_i + \alpha) \end{aligned} \quad (6)$$

where X_{ic0} is the initial position of the center of the circular leg in the fore/aft direction. The displacement of the hip in the vertical direction can be described as

$$\begin{aligned} Z_{ih} = & r_\omega - r_\omega \cos(\phi_t - \phi_i - \alpha) \\ & + r_\omega \cos(\phi_t - \phi_i - \alpha + \psi_0 - \psi_i) \\ & + (r_\omega - r_s) \cos(\phi_i + \alpha). \end{aligned} \quad (7)$$

Thus, the accelerations of the hind hip (\ddot{X}_{hh} , \ddot{Z}_{hh}) can be yielded by double derivation of (6) and (7) (i.e., $i = h$). By further importing the results into (4) and (5), respectively, the COM accelerations can successfully be represented as functions of variables (ϕ_h , ψ_h , α) and other model parameters.

Representations of the forces and torques shown in (1)–(3), (F_{xi} , F_{zi} , τ_i) as functions of three variables (ϕ_h , ψ_h , α) are described in this paragraph. On the torque side, because the hip torque τ_i is empirically generated by a brushed DC motor, it can be represented as

$$\tau_i = (V_i - k_b \dot{\phi}_i N_g) k_t N_g E_g / R \quad (8)$$

where V_i , k_b , N_g , k_t , E_g , and R are input voltage, electromotive force constant, gear ratio, torque constant, efficiency, and resistance of the motor, respectively. Basically, the output torque is a function of V_i and $\dot{\phi}_i$. On the force side, the leg is assumed to be massless because the leg mass in the RHex-style robot is relatively low in comparison with the body mass. Our robot has a mass of 6.2 kg, and each leg (half-circular Polyethylene and tire tread) has a mass of 0.068 kg. Thus, the mass of all the legs as a percentage of the robot's overall mass is 6.6%. This massless assumption allows the forces/torques acting on the leg to be derived by using static equations as shown in Fig. 2(c), where two free-body diagrams are constructed to extract the effect of the spring. The force equilibria yield

$$\begin{aligned} f_i &= F_{xi} \\ N_i &= F_{zi} \\ F_{xti} &= F_{xi} \\ F_{zti} &= F_{zi} \end{aligned} \quad (9)$$

where N_i and f_i are normal and friction forces on the ground, respectively, and F_{xti} and F_{zti} are horizontal and vertical forces acting on the torsional spring, respectively. The torsional spring

is assumed to have a linear relation between the torque τ_{ti} and the rotational displacement as

$$\tau_{ti} = K_t(\psi_i - \psi_0) \quad (10)$$

where K_t is the spring constant. By importing (9) and (10) into two equilibrium equations of moment, one with respect to the hip as shown in the left panel of Fig. 2(c) and the other with respect to the rotation joint of the torsional spring as shown in the right figure of Fig. 2(c), the unknown hip forces (F_{xi} , F_{zi}) can be represented as functions of the hip torque and the leg state as

$$\begin{aligned} F_{xi} &= \frac{(a_{4i} + a_{2i})\tau_i - a_{2i}K_t(\psi_0 - \psi_i)}{a_{1i}a_{4i} + a_{3i}a_{2i}} \\ F_{zi} &= \frac{(a_{1i} - a_{3i})\tau_i - a_{1i}K_t(\psi_0 - \psi_i)}{a_{1i}a_{4i} + a_{3i}a_{2i}} \end{aligned} \quad (11)$$

with

$$\begin{aligned} a_{1i} &= r_\omega + r_\omega \cos(\phi_t - \phi_i - \alpha + \psi_0 - \psi_i) \\ &\quad - r_\omega \cos(\phi_t - \phi_i - \alpha) + (r_\omega - r_s) \cos(\phi_i + \alpha) \\ a_{2i} &= r_\omega \sin(\phi_t - \phi_i - \alpha + \psi_0 - \psi_i) - r_\omega \cos(\phi_t - \phi_i - \alpha) \\ &\quad + (r_\omega - r_s) \sin(\phi_i + \alpha) \\ a_{3i} &= -r_\omega \cos(\phi_i + \alpha - \phi_t) + (r_\omega - r_s) \sin(\phi_i + \alpha) \\ a_{4i} &= r_\omega \sin(\phi_i + \alpha - \phi_t) - (r_\omega - r_s) \sin(\phi_i + \alpha). \end{aligned}$$

Equation (11) shows that the torque and forces of the hind hip (τ_h , F_{xh} , F_{zh}) are readily represented in the variables (ϕ_h , ψ_h , α) and other model parameters. In contrast, the torques and forces of the front hip (τ_f , F_{xf} , F_{zf}) and middle hip (τ_m , F_{xm} , F_{zm}) require further derivation to represent the leg state of the front and middle legs (ϕ_f , ϕ_m , ψ_f , ψ_m , $\dot{\phi}_f$, $\dot{\phi}_m$) with that of the hind leg. This can be done by utilizing the assumption of pure rolling motion of the legs and the geometrical relations among the hips. Using the middle leg as an example (i.e., $i = m$), the following equations hold:

$$\begin{aligned} X_{mh} &= X_{hh} + l_h \cos \alpha \\ Z_{mh} &= Z_{hh} + l_h \sin(-\alpha). \end{aligned} \quad (12)$$

By using (6) and (7), the unknowns ϕ_m and ψ_m can be solved simultaneously and represented in three selected variables (ϕ_h , ψ_h , α). Similarly, by using derivatives of (6), (7), and (12), the unknowns $\dot{\phi}_m$ can be represented by the state of these three variables as well. After replacing the leg state of the front and middle legs with that of the hind leg, the six forces shown in (11) are represented in the variables (ϕ_h , ψ_h , α) and other model parameters.

Finally, the computable EOM of the model can be formulated by importing the torques shown in (8), the hip forces shown in (11), and the COM acceleration shown in (4) and (5) into the EOM of the model shown in (1)–(3). Its state-space form can

be abstractly described as

$$\frac{d}{dt} \begin{bmatrix} \phi_h \\ \dot{\phi}_h \\ \psi_h \\ \dot{\psi}_h \\ \alpha \\ \dot{\alpha} \end{bmatrix} = \begin{bmatrix} \dot{\phi}_h \\ f_1(\phi_h, \dot{\phi}_h, \psi_h, \dot{\psi}_h, \alpha, \dot{\alpha}, V_i) \\ \dot{\psi}_h \\ f_2(\phi_h, \dot{\phi}_h, \psi_h, \dot{\psi}_h, \alpha, \dot{\alpha}, V_i) \\ \dot{\alpha} \\ f_3(\phi_h, \dot{\phi}_h, \psi_h, \dot{\psi}_h, \alpha, \dot{\alpha}, V_i) \end{bmatrix} \quad (13)$$

where functions f_1 – f_3 are simplified representations of the dynamic equations. With the I.C.s, the dynamic motion of the three-leg model can be started to simulate numerically via (13). Note that the I.C.s are specified in model body state (X_c , Z_c , α) for analysis, and they are mapped to (ϕ_h , ψ_h , α) only when numerical computation is performed.

The computation program is designed to start the simulation with I.C.s, where all the legs contact the ground, and to end when all the legs leave the ground. The transition condition where each leg loses ground contact is monitored and included in the program. The simulation runs recursively, and at each time stamp, the normal forces between legs and ground (N_f , N_m , N_h) shown in (9) are computed. When N_i equals 0, the leg is considered to be at take-off, and in computation, the force and torque interaction between this leg and the model body (τ_i , F_{xi} , F_{zi}) shown in (1)–(3) are set to 0. After all the legs are in take-off state, the model is in flight phase. The COM motion and body orientation are modeled as ballistic flight (i.e., projectile trajectory) and constant velocity model, respectively:

$$\begin{aligned} X_c &= X_{ct} + \dot{X}_{ct}t \\ Z_c &= Z_{ct} + \dot{Z}_{ct}t - \frac{1}{2}gt^2 \\ \alpha &= \alpha_t + \dot{\alpha}_t t \end{aligned} \quad (14)$$

where t , α_t , X_{ct} , and Z_{ct} are time, body pitch, and horizontal and vertical positions when the model takes off (i.e., I.C.s for flight phase).

III. DESIGN OF A LEAPING MANEUVER

The goal of this paper is to develop hurdling-like leaping behavior on an empirical robot with transition between tripod running. Therefore, the model behavior is developed to satisfy the following conditions: 1) The body state while running is regarded as the I.C.s for leaping; 2) the body state after leaping can be smoothly transitioned back to running, and here, the horizontal body landing posture (i.e., $\alpha = 0$) is the most critical factor; and 3) long-distance leap is desired. Note that the planar projection of tripod locomotion in the sagittal plane is identical to the proposed three-leg model; therefore, it is feasible to use the same model for leaping as well as transition to and from running without causing any inconsistency.

The motion of the model is numerically computed by importing the I.C.s and input motor voltage to the EOM of the model represented in state space as shown in (13). A leaping begins when the model lands on the ground right after its flight phase of running as shown in Fig. 3(a), and the body state of the model right before landing becomes the I.C.s for leaping.

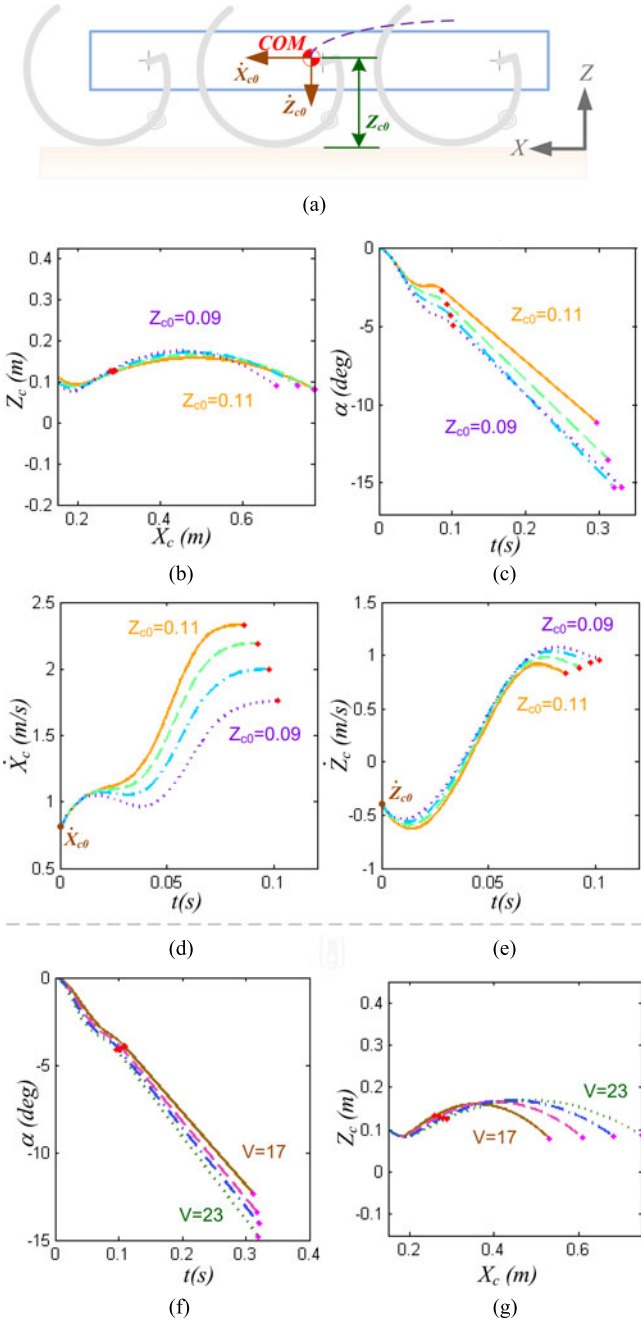


Fig. 3. Various body states of the model versus time in first-step leaping. (a) Sketch of the I.C.s. Subplots (b)–(e) with varying initial body height Z_{c0} (unit: m): (b) COM trajectory; (c) body pitch; (d) horizontal velocity; (e) vertical velocity. Red and magenta dots in (b) and (c) represent take-off and landing moments, respectively. Subplots (f) and (g) with varying supplying voltages (unit: volts): (f) body pitch; (g) COM trajectory.

The I.C.s have the following characteristics: 1) The initial body posture is horizontal without variation (i.e., α_0 and $\dot{\alpha}_0$ at zero) because when the model runs, variation of the body pitch is small. This behavior is also empirically observed on the robot experiments, where the pitch variation is less than 2° . 2) The legs have the same orientations (ϕ_i) because of the horizontal posture and uncompressed torsion springs. 3) The initial forward COM velocity (\dot{X}_{c0}) is determined by the landing condition,

and the initial forward COM coordinate (X_{c0}) is not critical. 4) The initial vertical COM velocity (\dot{Z}_{c0}) is determined by the landing condition. The initial COM height (Z_{c0}) can be varied by setting the leg orientation at a different configuration. 5) The legs are all in their natural configuration (ψ_0). Given the I.C.s described above, if the three ground-contact legs of the model are simultaneously driven with full power (i.e., providing full voltage as shown in (8)), the model can initiate the flight as shown in its COM trajectory in Fig. 3(b), which includes two portions: leaping phase (before the red dot, at least one leg touches the ground) and flight phase (between the red and magenta dots). The initial COM height Z_{c0} is varied in the figure since it is the only I.C. that is easier to manipulate than the other five I.C.s (i.e., α_0 , $\dot{\alpha}_0$, X_{c0} , \dot{X}_{c0} and \dot{Z}_{c0}). During flight, the body lifts only about 0.1 m during leaping. Thus, inadequate body pitch might cause a collision with the ground or obstacles. Fig. 3(c)–(e) plots the body state (body pitch, forward velocity, and vertical velocity) versus time. Fig. 3(c) clearly reveals an important fact: No matter at which COM height the model starts to thrust, the body pitch decreases (i.e., head goes up). This phenomenon is undesirable since 1) the possibility of collision between the back side of the robot and ground or obstacle increases significantly and 2) this posture is not adequate for the robot to transition back to running. This head-up phenomenon resulted from forces/torques acting on the body in a mainly clockwise direction. The force/torque plot of the model shown in Fig. 2(a) reveals that when the body pitch is close to 0° , the torques generated by the three horizontal forces (F_{xf} , F_{xm} , and F_{xh}) and vertical force of the middle leg (F_{zm}) to the body have smaller values than the other five forces/torques because of very short moment arms. As for the remaining five forces/torques, except for the vertical force of the hind leg (F_{zh}) which produces the counterclockwise torque, the vertical force of the front leg (F_{zf}) and three torques (τ_f , τ_m , and τ_h) all produce clockwise torques. The vertical forces are passively determined by model weight distribution. The effects of F_{zh} and F_{zf} cancel out each other. Their resultant effect on torque is not significant unless the body has a nontrivial tilted configuration or the applied torques have dramatically different magnitudes. Thus, the torques can be regarded as the main factor which results in the body pitching up. Fig. 3(f) supports this conclusion where less torque yields less pitch-up. However, Fig. 3(g) also reveals an undesired fact that the flying distance of the COM decreases more significantly with less applied voltage/torque. As a side note, the body pitch-up phenomenon also holds in the model with three linear spring legs, because the force/torque conditions of this model are not significantly different from the model with torsion spring legs. Thus, it is no simple manner for the current model with only three passive compliant legs to perform a leap within one stride and maintain horizontal body orientation.

Given that a head-up pitch of the model in first-step leaping is unavoidable, the second-step leap is investigated with a head-up I.C., the same configuration shown in Fig. 2(a). Fig. 4 plots various states with time when the robot starts to thrust with full power and initial COM height 0.095 m at different initial body pitches, varying from -7° to -12° . The figure reveals that the

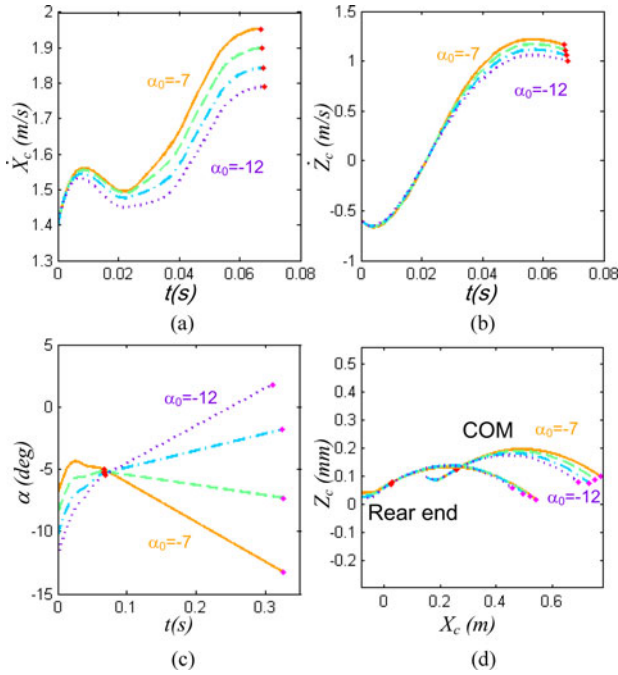


Fig. 4. Simulation of various body states versus time with varying initial body pitch α (unit: degrees) in second-step leaping: (a) horizontal velocity; (b) vertical velocity; (c) body pitch; (d) COM trajectory. Red and magenta dots represent take-off and landing moments, respectively.

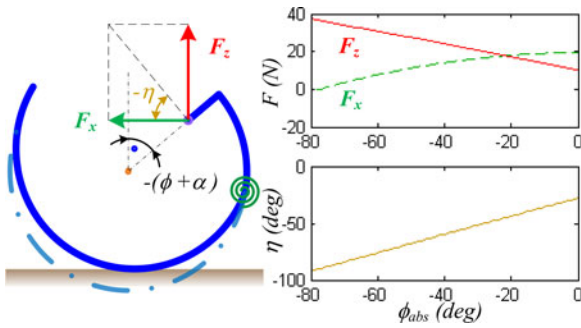


Fig. 5. Magnitude of the horizontal force (dashed green line) and vertical force (solid red line) components vary accordingly to the absolute leg orientation, $\phi_{abs} = \phi + \alpha$.

profiles of body pitch versus time can be dramatically different with different initial body pitches, and final body pitch could be dramatically different from its initial head-up condition. This phenomenon is desirable since it reveals that body pitch can be adjusted back to the desired horizontal status after leaping. A suitable initial body pitch can be selected to make the final body pitch close to horizontal for proper landing. The figure reveals that -10° is around the right range. The mechanism of body pitch alternation can be interpreted by the resultant forces/torques acting on the body. Fig. 5 plots the magnitudes of the forces versus the absolute leg configuration with respect to the ground, ϕ_{abs} , with given fixed spring compressions. The figure shows that the horizontal and vertical forces have different trends. Thus, if the body pitch α is negative (i.e., head up) as shown in Fig. 2(a), the absolute leg orientation with respect to

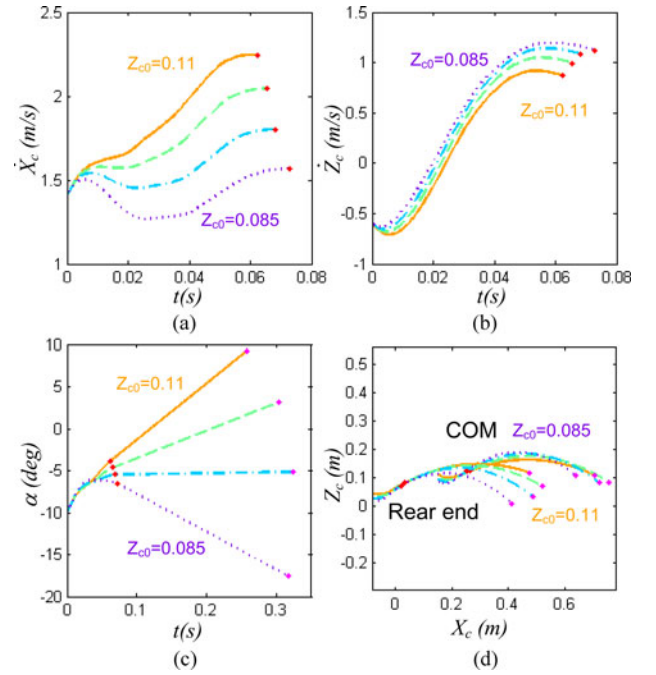


Fig. 6. Simulation of various body states versus time with varying initial body height Z_{c0} (unit: meters) in second-step leaping: (a) horizontal velocity; (b) vertical velocity; (c) body pitch; (d) COM trajectory. Red and magenta dots represent take-off and landing moments, respectively.

the inertial frame, ϕ_{abs} , of all three legs is different: The front leg has a larger horizontal force and the hind leg has a larger vertical force. As a result, the resultant torque acting on the body is sensitive to body pitch, and with the right selection, the body pitch can be adjusted back to nearly zero after leaping. Note that the forward and vertical velocities are plotted in Fig. 4(a) and (b), which provide the velocity transition during the leaping phase. The larger values are preferred since the end values (i.e., model take-off velocity) determine how far the model can fly in the subsequent ballistic flight phase. Since the variations are small and cause less effect, the parameter selection is judged according to the behavior of body pitch variation.

Besides body pitch, initial COM height can also be a maneuverable I.C. as that in the first-step leaping; therefore, its effect should be investigated as well. With the body pitch set to -10° , Fig. 6 shows various states over time when the robot starts to thrust with full power at different initial COM heights. Because the initial COM height changes the initial ϕ_{abs} , different initial COM heights also have direct effects on the profile of the body pitch during leaping, similar to the effect resulting from variation of the body pitch. Higher initial COM height yields a smaller leg configuration ϕ_{abs} and larger forward force; thus, the take-off forward velocity can be made higher as shown in Fig. 6(a). In contrast, lower initial COM height favors vertical force, which yields larger take-off vertical velocity as shown in Fig. 6(b). The resultant take-off velocity vector determines the flying trajectory as shown in Fig. 6(d), where higher initial COM height yields flight with longer distance. However, the body pitch is also sensitive to the initial COM height, and an

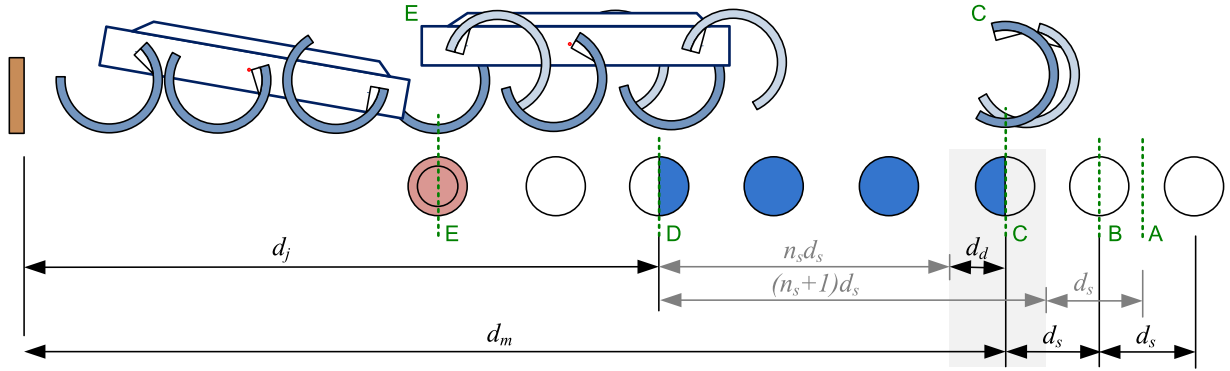


Fig. 7. Illustrative sketch of overall running to leaping transition of the robot. Brown rectangle represents the obstacle. Circles represent the positions of the front leg of the ground-contact tripod when it poses vertically down (i.e., at 0°). When the robot detects an obstacle with measurements less than $d_j + (n_s + 2)d_s$ (position A), the distance to the obstacle, d_m , is computed during the next tripod stance (between positions B and C). Then, the robot runs with the modified stride length for the next three strides (between positions C and D, marked with blue circles). After one stride of ordinary tripod running to yield consistent I.C.s, the robot performs leaping behavior (position E).

adequate initial COM height should be selected, for example, around 0.095 m, to yield horizontal flight.

The morphology of the model determines its achievable dynamic behavior. In general, if the legs of the model have sufficient DOFs for maneuvering body posture and have large instantaneous power for rapid body/leg state changes, the model may be able to transition its behavior from running to leaping in one stride, as animals do. Here, the design of the model is inspired by the empirical RHex-style robot for experimental evaluation. The RHex-style robot is famous for its simple mechanical and actuation structure yet is capable of performing versatile and dynamic behaviors [27], [31], [45], [46]. However, the simple structure also prevents the system from being easily maneuverable. We experienced this issue in our previous development of a high-step climbing behavior on the same robot [40], where the dedicated leg trajectory planning and body maneuver is crucial for successful climbing. The analyses in Sections II and III reveal that the current three-leg model has difficulty transitioning from running to leaping in one step. The body pitching up is the critical and undesired behavior when the model initiates its leap with a horizontal posture. If the legs are oriented at the very beginning of the leap to have different initial ground contact timings and force interactions, the resulting behavior may be different. However, we did not investigate this approach because it seems a challenge to configure the body posture and inject enough energy to the model in a brief time for leaping (i.e., less than 80 ms). Instead, the second-step leaping is investigated and serves as the main leaping step. The first step is utilized for adjusting the body posture (i.e., pitch) to the right configuration and for speeding up the forward velocity. The two-step leap has several other benefits in empirical implementation. The flight phase of the first-step leaping allows the robot to synchronize the phases of all six legs; therefore, the body can leap with full thrust from all legs in the second-step leap. This thrust strategy is very helpful, especially for current ordinary walking/running robots that usually do not have high power density. In addition, the thrust from all legs reduces the yaw and roll variations on the robot.

The overall leaping behavior can now be constructed based on the above analysis. After the aerial phase of an arbitrary running stride, the body lands on the ground with a horizontal posture and selected COM height. At this instant, the first-step leaping is initiated and the legs provide full thrust to the body, and the robot moves according to the trajectory shown in Fig. 3(b). During the flight, the legs are synchronized and prepared to land with the desired COM height and body pitch. After touching the ground, all legs again provide full thrust and initiate the second-step leaping, which makes the robot move according to the trajectory shown in Figs. 4(d) or 6(d). Note that the motor torques for the second-step leaping in computation shown in (1) are doubled because the number of legs for actuation in the empirical system are doubled. During the second-step leap process the first, middle, and hind legs take off in sequence, and each has 37, 55, and 67 ms of contact with ground. In the model, all three legs contact the ground at the very beginning; therefore, 67 ms is the stance time of the leaping. As a side note, because the I.C.s of the first-step leap can be set to zero, the development is also suitable for the robot leaping from a static posture.

Note that although the detailed modeling work may appear to be suitable only for the RHex-style robot with half-circular legs, the methodology of model-based behavior development is actually general and can be applied to other systems. For example, if a robot has linear compliant legs with point ground contacts, its leaping behavior can be developed by first constructing the reduced-order model with linear spring legs, and then investigating the behavior of the model by parameter variation as described in this section. More specifically, for the modeling part, the following equations should be modified: Equations (6) and (7) that define the detail configuration between the hip and ground, along with equations (9)–(11) that define the force property of the leg. The other equations can be applied to the new model directly. Since the linear spring leg has a simpler formulation than the R-SLIP leg, the modeling work is expected to be much simpler. In addition, we also expect that the behavior of this model is likely to have similar trends as the developed one

because the force/moment interaction between the robot body and the ground shown in Fig. 2(a) seems to be similar. The rolling contact versus point contact may yield some difference, but this is not expected to be significant. Of course, the precise performance of the model with linear spring legs will still rely on quantitative and thorough analysis of the revised model, but the behavior trend can be revealed in the model with close similarity. For the robot with high-DOF legs, the results of this work may be applicable if its legs are controlled to act like passive springs. This is indeed the fundamental strategy used in biological system models, which have articulated limbs but with very simple motion such as SLIP [33], [34]. Note that in this case, the mass percentage of the legs to the overall body may not be trivial, and a leg model that has better morphology mapping to the original leg may be needed.

More broadly, this study proposes a methodology of developing a dynamic gait through utilization of a reduced-order model. By defining and using a “template” [36] for gait development, the smaller parameter space allows us to investigate the effects of the parameters as well as find the adequate leg motion sequence, thus achieving the desired model behavior. Through this model-based approach, the dynamics of the system and its underlying mechanics can be revealed as well, and this is hard to achieve by gait tuning or optimization methods.

IV. TRANSITION FROM RUNNING TO LEAPING

Leaping is often desired to be initiated and transitioned from running at a specific position such as hurdling or leaping over a ditch. In this case, the robot should be capable of reaching a specific position with the right body state in order to provide the correct I.C.s for leaping. To achieve this, the robot should know the distance from its current position to the position for leaping, and it should be capable of adjusting its stride length from stride to stride.

The general methodology of the overall running to leaping transition can be formulated as follows, using Fig. 7 as the accompanying illustrative diagram. Assume the robot has one tripod posing vertically down at point D. This point is the position where the leaping process initiates. The distance d_j is the distance where the process occurs. Following this notation, the stride is defined as the interval that starts when one tripod poses vertically down and ends when the next tripod poses in the same posture. If the distance from the current position to point D at an arbitrary instant when one of the tripods poses vertically down is fortunate enough to be an integer multiple of the stride length, d_s , no stride length adjustment is required. In general a discrepancy distance $d_d < d_s$ exists, and regulation is needed. This discrepancy can be evened out by increasing or decreasing the stride length of the robot. Assuming the stride length can be adjusted to increase $100 p_i$ percentage or decrease $100 p_d$ percentage per stride, the minimum distance required for regulation is

$$d_s(n_s + 1) \text{ with } n_s = \text{ceil}(1/(p_i + p_d)) \quad (15)$$

where n_s is the minimum number of strides required for regulation, and $\text{ceil}()$ is a function that rounds the element up to the

nearest integer greater than or equal to the element inside. Set d_m as the distance to the obstacle where the regulation begins as shown in Fig. 7, bounded within

$$d_j + d_s n_s < d_m < d_j + d_s(n_s + 1). \quad (16)$$

With this definition, the discrepancy d_d can be computed as

$$d_d = \text{rem}(d_m - d_j, d_s) \quad (17)$$

where $\text{rem}()$ yields the remainder after division of the former value by the latter. The adjusted stride length \tilde{d}_s can be formulated as

$$\begin{aligned} & \text{If } d_d/d_s \leq p_i n_s \\ \tilde{d}_s &= d_s + d_d/n_s \\ & \text{else} \\ \tilde{d}_s &= d_s - (d_s - d_d)/(n_s + 1). \end{aligned} \quad (18)$$

When the “if” condition holds, the stride length increases to even out the distance discrepancy (i.e., n_s strides). Otherwise, the stride length decreases and one more stride is required (i.e., $n_s + 1$ strides). In both cases, the robot uses the modified stride length computed in (18) to move $\tilde{d}_s n_s + d_d$ and reaches position D, as shown in Fig. 7. Note that the discrepancy is evened out by all the strides during regulation, not in one stride, to make the transition less dramatic.

The methodology described in the previous paragraph requires the distance d_m as the prior information, and this can be obtained by the distance measurements within several strides before the stride regulation. Assume a range sensor exists which is capable of continuously sensing the front side during ordinary running. When the sensor detects an obstacle with distance measurements less than $d_j + d_s(n_s + 2)$, the program for d_m determination is initiated. The distance is computed based on the measurements during the slow-swing phase of the next tripod motion:

$$d_m = \text{mean}(d_i - \dot{X}_c(1/f_s - (i-1)/f_c)), i=1\dots n \quad (19)$$

where f_s and f_c are the frequencies of stride and control loop, respectively. The symbol i is the index of the control loop, and $i = 1$ and $i = n$ represent the moments when the tripod poses vertically down and at some angle afterward in one specific stride right before stride regulation. Equation (19) averages several measurements for better distance estimation, yet it yields the distance when one of the tripods poses vertically down as required by the algorithm described in the previous paragraph.

With the strategy described in the previous two paragraphs, the algorithm for stride length regulation in the RHex-style robot can be quantitatively programmed. The legs of the robot in the original tripod locomotion move according to the preset Buehler Clock [27], which parameterizes the leg motion by four parameters, including period, time of slow-swing phase, angle of slow-swing phase, and offset angle. Because angle of slow-swing phase basically determines how much the body can be pushed forward in this specific period, it is directly linked to the stride length, unless the foot slippage phenomenon is severe. In addition, altering other parameters such as period and time of

slow-swing phase is more difficult owing to the leg coordination issue and stability consideration. Therefore, adjusting the angle of the slow-swing phase to regulate the stride length appears to be an adequate choice. Empirical investigation showed that relation between the stride length (in meters) and angle of slow-swing phase, φ_s (in degrees), can be approximated by an affine function (unit cm):

$$\tilde{d}_s = 0.176 \varphi_s + 4.565. \quad (20)$$

This approximation is valid for stride length between 0.11 and 0.17 m. With the default stride length $d_s = 0.125$ m, the achievable percentages of stride length increasing and decreasing are $p_i = 0.36$ and $p_d = 0.12$, respectively. Following that, equation (11) yields $n_s = 3$. Because in this particular setting, the ceil() condition largely pulls the original fraction of 2.08 to 3, increasing the stride length can already cover all possible distance discrepancies d_d (i.e., $p_i n_s = 1.08 > 1$). Thus, when the discrepancy exists, $d_d \neq 0$, it will be evened out by increasing the stride length. For example, if $d_d/d_s = 0.66$, $\tilde{d}_s = 1.22d_s$ for three consecutive strides. As for the measurement of d_m , an infrared (IR) range sensor is utilized and mounted on the front of the robot. Note that in the current setup, the sensor can detect the existence of the obstacle but not the ditch, and in the former case, the sensor still cannot reveal the obstacle's dimensions. A precise determination of whether the leaping behavior should be initiated or not requires robust and delicate environment recognition, and this aspect is beyond the scope of this study. Here, the effort on the sensor side is minimized and focuses on the strategy of how to perform the transition when the obstacle is detected. Along with Fig. 7, the overall running to leaping transition in the empirical RHex-style robot is described as an example of algorithm utilization. During ordinary running, the IR sensor continuously senses the front side of the robot. When the robot detects an obstacle with measurements less than $d_j + 5d_s$ (position A), the distance to the obstacle, i.e., d_m , is computed during the next tripod stance (between positions B and C). Then, the robot runs with the modified stride length for the next three strides (between positions C and D). After one stride of ordinary tripod running to yield consistent I.C.s, the robot performs leaping behavior (position E).

V. EXPERIMENTAL EVALUATION

The RHex-style robot shown in Fig. 1(a) was used to evaluate the performance of the proposed development of leaping behavior. The robot has a length of 0.47 m, width of 0.37 m, standing height of 0.14 m, and leg diameter of 0.13 m. It has a mass of 6.2 kg, and each leg (half-circular Polyethylene and tire tread) has a mass of 0.068 kg. The robot COM is not located at the exact geometric center of the body, but slightly toward the front side, as shown in Fig. 1(b). The mass moment of the robot approximates $0.1258 \text{ kg}\cdot\text{m}^2$ according to the computer-aided design model of the robot. The robot has a real-time embedded control system (sbRIO-9602, National Instruments) running at a 500-Hz sampling rate, and it also has various onboard sensors. The detailed specification of the robot can be found in [40]. The IR range sensor utilized in this study is from Sharp (GP2Y0A710).

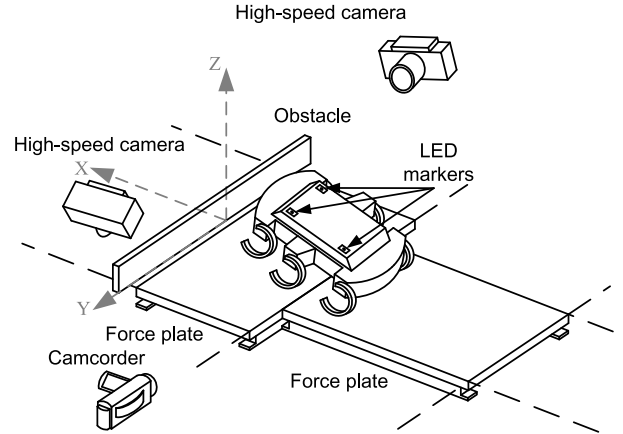


Fig. 8. GTMS, the experimental setup for collecting quantitative leaping data of the robot.

The experimental data were collected, while the robot leaped within the ground truth measurement system (GTMS), shown in Fig. 8. The system has two high-speed cameras (A504k, Basler) installed on the top right and left sides of the experimental area to capture three LED markers mounted on top of the robot. The 3-D positions of the markers can be reconstructed by two synchronized images captured by the high-speed cameras, running at 250 Hz. The resolution is within ± 1 cm in a runway about 1.5 m long and 0.5 m wide. The COM trajectories and the body orientations versus time were recovered by the computed 3-D coordinates of the three markers. The force plate (4060-07-1000, Bertec) was placed on the runway to record the force interaction between the robot and the ground. A camcorder (HDR-XR350, SONY) recorded the robot's leaping motion from a side view.

The simulation results of the three-leg model shown in Section III use the robot's parameters and characteristics as a reference; therefore, the trajectory designed in the model can directly be deployed on the robot. The parameters of the model that are directly imported from the robot include mass, inertia, robot dimensions, motor model, and running body state as I.C.s of leaping. The parameters of the model that do not have direct mapping to the physical robot are the leg properties, including the position and stiffness of the torsion spring. The morphology of the legs of the three-leg model or the R-SLIP model is actually constructed based on the solid mechanical characteristics of the half-circular material with linear elastic and isotropic properties, and the details are described in [42]. In short, by using the strain energy method (i.e., Castigliano's Theorem), the linear and approximated planar relation between the forces and the deformations of the leg can be obtained (i.e., stiffness matrix). The eigendecomposition of the stiffness matrices of the material with different contact points further suggest that the resultant compliant behavior of the half-circular material can be approximated by a rigid two-link model with a torsion spring in between, yielding the morphology of the R-SLIP leg. The position of the torsion spring is approximately located $35\text{--}65^\circ$ on the circular rim and below the hip, and 35° was adopted. On the other hand, the stiffness of the torsion spring used in the model

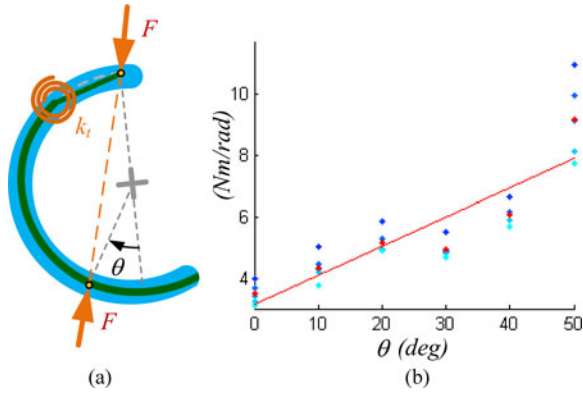


Fig. 9. Force-deflection measurements of the robot leg (blue thick curve) and its mapping to the torsion spring stiffness of the model.

was estimated based on the compression force measurements of the real robot legs as shown in Fig. 9(a). The force-deflection relation of the empirical leg was measured at six contact points 10° apart, and at each contact point, the force data were collected with five different deflection levels. All these force-deflection data were further transformed into the torque-angular deflection data as shown in Fig. 9(b), and the details can be found in [42]. Its linear approximation was set as the stiffness of the torsion spring on the leg. With the derived spring stiffness and position, the three-leg model can indeed be regarded as the reduced-order model of the original complex robot. The modeling work described in Sections II and III suggests an adequate leg maneuver sequence, which would initiate the leaping behavior. Because the robot does not have a body state or ground contact estimation system with a high enough bandwidth to provide sensory feedback for a closed-loop algorithm in this extreme dynamic leaping (the stance phase takes less than 70 ms), the timing-based motion sequence is programmed on the robot. The stride length regulation described in Section IV is reactive, and after the robot reaches the desired position for leaping, it starts to leap by deploying the leg maneuver sequence developed in Section III.

Fig. 10 shows seven experimental results of the robot running toward an obstacle with stride length regulation. In the experiments, the robot started with different distances to an obstacle (spanning around 18-cm difference), and it reached the same position with a specific distance to the obstacle, d_j . The standard deviation of d_j is 0.011 m, equal to 1.3% error of the distance. In addition, because the robot did not alter its stride period during stride regulation, the robot arrived at the position for leaping with several fixed timings, which were dependent on the initial distance of the robot to the obstacle (i.e., the required number of strides).

Fig. 11 plots five experimental results of COM trajectories measured by the GTMS when the robot leaped over the 0.095 m obstacle, which is larger than the ground clearance of 0.082 m of the robot while standing. Fig. 11(a) and (b) shows 3-D trajectories and its projected trajectories in the XZ (sagittal) plane, respectively. The COM trajectories of the robot in the sagittal plane are quite consistent and have little deviation among each

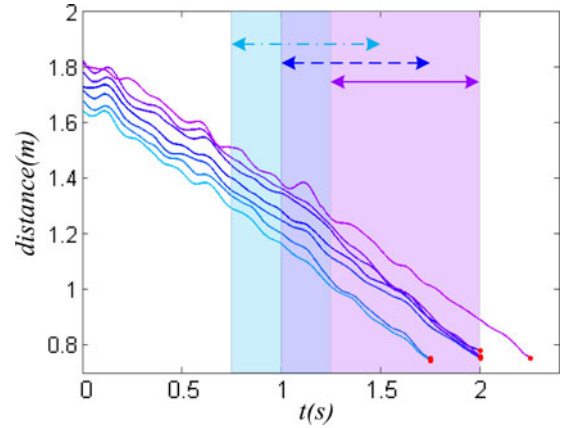


Fig. 10. Changing distance of automatic adjustment of stride length in different initial locations. Red points are the position one stride before the robot jumps and the distance should be $d_j - d_s$.

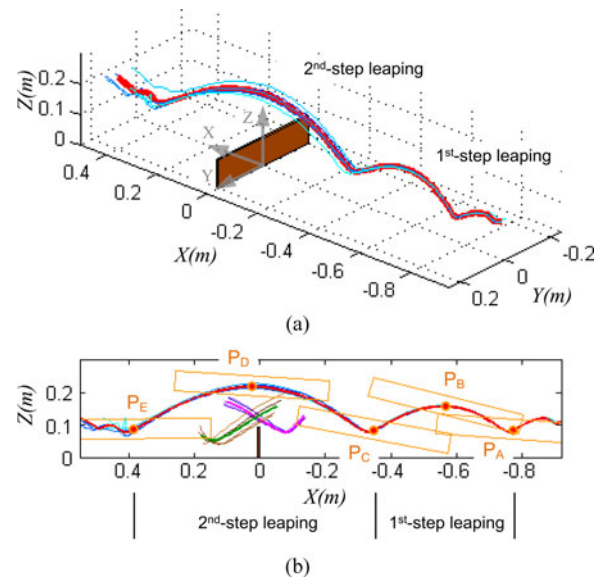


Fig. 11. Robot COM trajectories of leaping behavior measured by GTMS. (a) Three-dimensional plot. (b) Sagittal-plane plot. The red curve represents the averaged COM trajectory of five experimental runs (blue curves). The purple and brown curves depict the front and rear hip trajectories in take-off period and landing period, respectively.

other. With the same forward positions (x -coordinates), the average standard deviations of the robot's first-step and second-step leap in the vertical direction (z -coordinate) are 1.8 and 4.8 mm, respectively. Because 1) the performance of the first-step leap affects that of the second-step leap, and 2) the motion of the second-step leap is more dramatic, it is expected that the standard deviation of the second-step leap is larger than that of the first-step. The standard deviations are only 1.2% and 3.3% of the COM height; therefore, the leaping behavior of the robot is repeatable and quite consistent. The averaged traveling distances in the first-step leap (computed by the distance between positions P_A and P_C) and in the second-step leap (computed by the distance between positions P_C and P_E) are 0.43 and 0.74 m, respectively. Therefore, the thrust of all six legs in the

second-step leap can indeed increase the leaping performance. The flying distance of the second-step leaping equals to 157% of the body length, i.e., 0.47 m. Fig. 11(b) also plots the body orientations at various positions and trajectories of the front and rear hips (purple and brown curves, respectively). Owing to the consistent COM and body pitch profiles, the trajectories of these two hips are also consistent; therefore, the robot can successfully leap over obstacles with very tight clearance. It confirms that the body pitch is crucial in this hurdle-like locomotion as described in the trajectory development shown in Section III. The R value between the robot's flying trajectory and the projectile trajectory is 0.9982, which indicates that the ballistic model for the robot in flight is reasonably correct. Fig. 11(a) also reveals that, in practice, the robot has lateral deviation owing to unequal propulsion forces generated by the left or right legs. Nonetheless, the deviation of 0.042 m is considered small when compared with the overall leaping distance of around 1.2 m.

Fig. 12 plots various states versus time in both model analysis and in the experiment, while the robot leaped over the obstacle (the second-step leap). Detailed notations are described in the figure caption. The model can predict well the behavior trend of the experiment. For example, the forward and vertical velocities in general increase. The body pitch increases (toward an even posture) and body pitch angular velocity decreases as expected. As for the vertical displacement, the valley-like motion is also captured by the model. As for the force profiles shown in Fig. 12(f), the model shows the right trends to the empirical behavior, and more than 50% of the time the model trends lie within the standard deviations of the experimental results. There exists some discrepancy between the model analysis and the experimental results. In addition to the GTMS resolution, this discrepancy mainly results from the unknown effects of several complicated and hard-to-model empirical factors such as the complex leg deformation pattern, slippage during ground contact, the assumption of massless legs in the model, etc. As for the first factor, the leg of the three-leg model is purely elastic and has only one rotational DOF. In contrast, the half-circle leg of the robot is made by polyethylene and has a continuously deformable structure with mixed elastic, plastic, and damping effects. We have run the free vibration test of the leg and checked its deformation response, and we found that the response is far from the linear model with elastic and damping component (i.e., adding a viscous damper to the torsional joint). In addition, the response does not linearly correspond to the magnitude change of the I.C.s. Therefore, it is challenging to have two systems yielding the same force-deformation pattern, especially when the leg is utilized in the leap behavior where large forces are involved. Ground slippage is another cause of the discrepancy. We did observe slippage in the recorded images, especially when the leg is close to take-off (with less friction force) because at this moment, the normal force is small, but the hip torque remains at a similar magnitude. Note that if slippage between the leg and ground is allowed, the DOFs of the model would double from 3 to 6, which greatly increases complexity of analysis. The assumption of massless legs in the model may also lead to some discrepancy. Although the leg mass is small in comparison with the total robot mass, it causes two unmodeled effects.

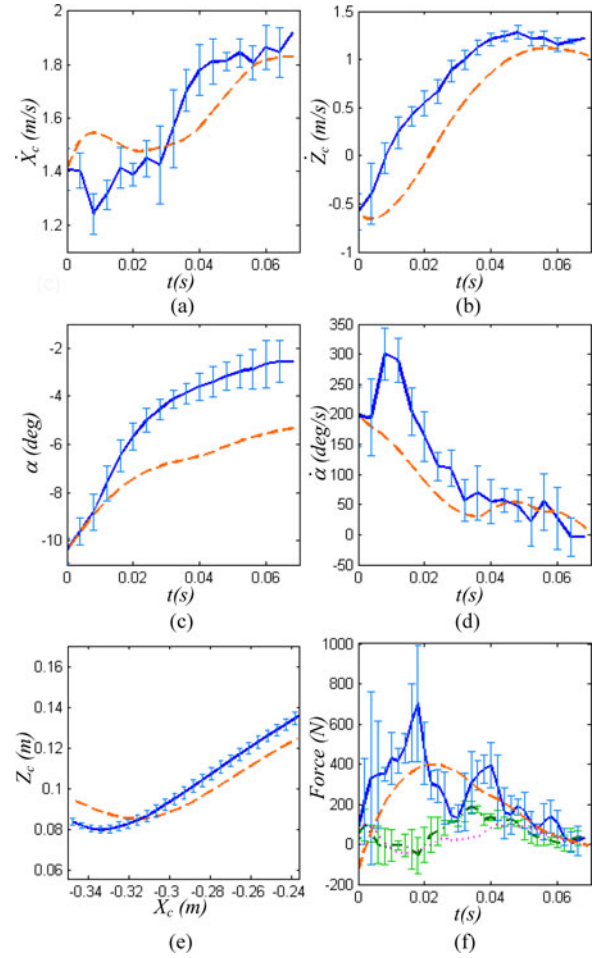


Fig. 12. Various states versus time in model analysis (dashed orange curve) and in experiments (solid blue curve), while the robot leaped over the obstacle (the second-step leap), including (a) horizontal velocity, (b) vertical velocity, (c) pitch angle, (d) pitch angular velocity, (e) COM trajectory, and (f) ground reaction forces. Dark blue [and dark dash-dotted green in (f)] and light blue [and light green in (f)] curves represent means and standard deviations of the experimental runs. Dashed orange [and dotted pink in (f)] curves represent the data yielded from the model analysis shown in Sections II and III. In (f), blue/orange curves and green/pink curves represent vertical and horizontal forces, respectively.

One is the contact impact at the beginning of the leap, when the robot touches down just after the flight phase of running. This can be observed in Fig. 12(f) with nonzero touchdown forces. The other is pitch disturbance when the leg swings, especially for the flight phase where the legs perform fast motion and the time duration is long. The pitch and roll variations result in (and result from) different contact conditions of all six legs. The impact and unsynchronized ground contact of the legs mainly alter the forward/vertical velocities as well as the body pitch rates of the robot close to the onset (the first 20 ms) of leaping. This is the main source of the discrepancy of body pitch. Note that the leaping event happens very fast (only taking 70 ms) and is extremely dynamic; therefore, a very delicate model is required if it is desired to decouple the discrepancy caused by these various reasons. This requires substantial work and is currently under investigation. Although some quantitative

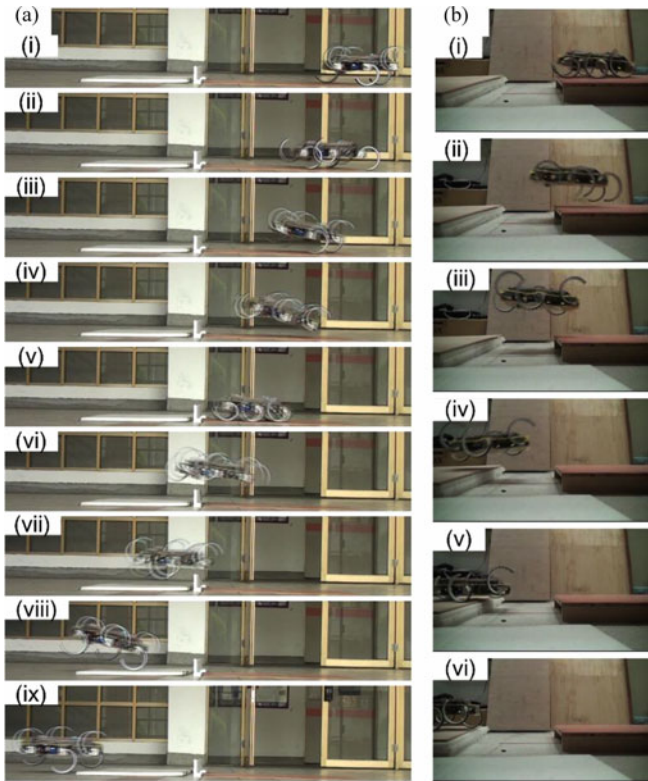


Fig. 13. Leaping of the robot. (a) Leaping over an obstacle (sequence images). (b) Leaping over a ditch.

discrepancy exists between the model and the empirical system, the discrepancy is quite small in comparison with the size of the robot and scale of the motion [1.2 m, from position P_A to P_E shown in Fig. 11(b)]. For example, the differences of final velocities are around 0.1 m/s, of pitch angle is 3° , and of vertical COM trajectory is within 0.01 m.

Fig. 12 also shows that duration of ground contact in the second-step leaping is only about 70 ms. This fact reveals the dynamic nature of the leaping behavior since all the states should change accordingly to generate a successful leap. The overall success rate of the robot leaping over an obstacle is 80%. It failed when the front or back side hit the obstacle, which was mainly caused by the variation of body pitch. The real-time pitch control is a good direction for further development. This will be a complete but separate piece of work because various issues for high-speed sensory, mechatronic, computational, and actuation strategy must be addressed.

Fig. 13(a) shows sequential images extracted from a video recording of the robot leaping over an obstacle. In the beginning, the robot ran toward the obstacle (i). Then it started the leaping behavior (ii), and took off for the 1st-step leaping (iii). During ballistic flight, two tripods were synchronized (iv), preparing for the landing with the correct body pitch and vertical COM height (v). Then, the robot initiated the second-step leaping and flew over an obstacle (vi) and (vii). Next, the robot landed on the ground (viii) and resumed running behavior (ix). The original movies are available as media extensions associated with this

paper. Fig. 13(b) shows sequential images extracted from a video of the robot flying over a ditch 0.4 m wide. Note that because the current range sensor cannot sense the distance from the robot to the ditch, the automatic stride length regulation was turned OFF, and the leaping was programmed to automatically initiate at a certain time stamp. This video is merely used for demonstrating the unique locomotion capability of leaping where other gaits are not applicable.

Comparing the empirical system with complex behaviors, the model described in Section II may be overly simple. However, it preserves the essential characteristics and behaviors of the empirical system; therefore, it can be utilized to predict the behavior of the empirical system. More importantly, it did serve to guide leaping behavior development. Before developing this model, we had tried to empirically design the leg trajectories for leaping but failed owing to the highly dynamic nature of this specific behavior. By using the three-leg model that reduces the DOFs of the complex system to merely three, the formulation of the model as well as the numerical investigation became feasible. Through the process, those factors critical to the behavior were found, and the underlying dynamic (force/moment) interaction of the model/robot to the ground was revealed. The development of leaping behavior through the three-leg model is not a trivial task, but this model-based methodology indeed provides a clear and feasible path toward development of a dynamic gait.

VI. CONCLUSION

We report on the methodology of developing dynamic leaping behavior in a hexapod robot through a model-based approach. To be free from the complex dynamics of the original platform as well as to generalize the behavioral development for wider applications, a planar three-leg model was developed to investigate the characteristics of leaping dynamics. The model is composed of a rigid body and three massless compliant legs, and it has 3 DOFs which can be roughly mapped to the three-planar state of the robot's COM, including vertical and horizontal motions as well as body pitch. The virtual leg of the R-SLIP model is utilized as the legs of the three-leg model, which has a better characteristic match to the empirical legs on the robot. Through analysis of the three-leg model with initial running conditions, we find that in the first-step leaping, the COM height during take-off is the only parameter easier to be tuned and programmed on the robot: No matter which height is chosen, the body pitches up and this state is sensitive to the COM height during take-off. In the following investigation with pitched-up body as the initial configuration for the second-step leaping, we found that both the body pitch angle and the COM height during take-off determine the final configuration of the model. With parameters selected from model analysis, the model can land on the ground with a horizontal posture, which is easier for transitioning back to running. As a result, the overall leaping is composed of two steps, where the first-step is utilized for 1) adjusting the body pitch to the right configuration, 2) synchronizing the phases of all six legs, and 3) speeding up the forward velocity. Consequently, the body can adequately leap with full thrust from all legs and with correct landing posture in the second-step leap. In

addition, the robot's transition from running to leaping involves not only using the running state as the I.C. for leaping, but also adjusting the model's stride conditions in order to leap at the correct position. We formulated the strategy, which gradually adjusts the stride length of the model. If the model is capable of larger stride length change per stride, the distance, time, and number of strides for transition can be reduced.

The developed leaping behavior and its transition from running in the three-leg model are empirically implemented on the RHex-style robot and experimentally evaluated. The IR range sensor is utilized to detect the presence of the obstacle and its distance to the robot; therefore, the robot is capable of correctly adjusting its stride length and arriving at an adequate position for initiating leaping behavior. The whole process is fully autonomous. Experimental results show that the leaping behavior of the robot is consistent, where the averaged and normalized standard deviations (i.e., divided by the COM height) of the first-step and second-step leaps are 1.2% and 3.3%, respectively. The robot can leap over a 0.095-m-high obstacle with flying distance 0.74 m, equal to 157% of body length and more than five times its leg length. The robot can also leap over a 0.4-m ditch, equal to 70% of body length and more than three times its leg length. By comparing the experimental results with the model analysis, the model correctly catches the trends of state transition during leaping. The quantitative discrepancy mainly results from the ignorance of several complicated and hard-to-model empirical effects such as the complex leg deformation pattern, slippage during ground contact, and assumption of massless legs in the model. Considering the size of the robot and the scale of its locomotion, the discrepancy is quite small. More importantly, the model indeed serves as a guide for the development of leaping behavior.

We are in the process of introducing a sensory feedback mechanism for leaping behavior. In addition to the algorithm side, this goal requires mechatronic revision of the robot for high-speed sensory input, large computation capability, and high-power actuation output. At the same time, the sensory system for detection and recognition of surroundings is also under development, to provide for autonomous gait selection and transition in a more thorough manner.

MEDIA EXTENSIONS

1. Leap (obstacle).mpg The robot leaps over an obstacle.
2. Leap (ditch).mpg The robot leaps over a ditch.

REFERENCES

- [1] M. Kovac, M. Fuchs, A. Guignard, J. C. Zufferey, and D. Floreano, "A miniature 7g jumping robot," in *Proc. IEEE Int. Conf. Robot. Autom.*, 2008, pp. 373–378.
- [2] J. G. Zhao, J. Xu, B. T. Gao, N. Xi, F. J. Cintron, M. W. Mutka, and L. Xiao, "MSU jumper: A single-motor-actuated miniature steerable jumping robot," *IEEE Trans. Robot.*, vol. 29, no. 3, pp. 602–614, Jun. 2013.
- [3] M. Noh, S. W. Kim, S. An, J. S. Koh, and K. J. Cho, "Flea-inspired catapult mechanism for miniature jumping robots," *IEEE Trans. Robot.*, vol. 28, no. 5, pp. 1007–1018, Oct. 2012.
- [4] U. Scarfogliero, C. Stefanini, and P. Dario, "The use of compliant joints and elastic energy storage in bio-inspired legged robots," *Mech. Mach. Theory*, vol. 44, pp. 580–590, Mar. 2009.
- [5] F. Li, W. T. Liu, X. Fu, G. Bonsignori, U. Scarfogliero, C. Stefanini, and P. Dario, "Jumping like an insect: Design and dynamic optimization of a jumping mini robot based on bio-mimetic inspiration," *Mechatronics*, vol. 22, pp. 167–176, Mar. 2012.
- [6] R. Niiyama, A. Nagakubo, and Y. Kuniyoshi, "Mowgli: A bipedal jumping and landing robot with an artificial musculoskeletal system," in *Proc. IEEE Int. Conf. Robot. Autom.*, 2007, pp. 2546–2551.
- [7] J. M. Morrey, B. Lambrecht, A. D. Horschler, R. E. Ritzmann, and R. D. Quinn, "Highly mobile and robust small quadruped robots," in *Proc. IEEE/RSJ Int. Conf. Intell. Robots Syst.*, 2003, pp. 82–87.
- [8] B. G. A. Lambrecht, A. D. Horschler, and R. D. Quinn, "A small, insect-inspired robot that runs and jumps," in *Proc. IEEE Int. Conf. Robot. Autom.*, 2005, pp. 1240–1245.
- [9] BostonDynamics. *SandFlea—Leaps Small Buildings in a Single Bound*. (2014). [Online]. Available: http://www.bostondynamics.com/robot_sandflea.html
- [10] S. A. Stoeter and N. Papanikolopoulos, "Autonomous stair-climbing with miniature jumping robots," *IEEE Trans. Syst. Man Cybern. B, Cybern.*, vol. 35, no. 2, pp. 313–325, Apr. 2005.
- [11] S. A. Stoeter and N. Papanikolopoulos, "Kinematic motion model for jumping scout robots," *IEEE Trans. Robot.*, vol. 22, no. 2, pp. 397–402, Apr. 2006.
- [12] G. M. Song, K. J. Yin, Y. X. Zhou, and X. Z. Cheng, "A surveillance robot with hopping capabilities for home security," *IEEE Trans. Consum. Electron.*, vol. 55, no. 4, pp. 2034–2039, Nov. 2009.
- [13] R. Armour, K. Paskins, A. Bowyer, J. Vincent, and W. Megill, "Jumping robots: A biomimetic solution to locomotion across rough terrain," *Bioinspiration Biomimetics*, vol. 2, pp. S65–S82, Sep. 2007.
- [14] Y. Sugiyama and S. Hirai, "Crawling and jumping by a deformable robot," *Int. J. Robot. Res.*, vol. 25, pp. 603–620, May/Jun. 2006.
- [15] H. C. Wong and D. E. Orin, "Dynamic control of a quadruped standing jump," in *Proc. IEEE Int. Conf. Robot. Autom.*, 1993, pp. 346–351.
- [16] S. A. Bowling, "Jump in the Horse" *Animal Locomotion*, 2014. [Online]. Available: <http://bowlingsite.mcf.com/Movement/HJump.html>
- [17] P. Chatzakos and E. Papadopoulos, "Bio-inspired design of electrically-driven bounding quadrupeds via parametric analysis," *Mech. Mach. Theory*, vol. 44, pp. 559–579, Mar. 2009.
- [18] I. Poulakakis, E. Papadopoulos, and M. Buehler, "On the stability of the passive dynamics of quadrupedal running with a bounding gait," *Int. J. Robot. Res.*, vol. 25, pp. 669–685, Jul. 2006.
- [19] M. M. Ankarali and U. Saranlı, "Control of underactuated planar pronking through an embedded spring-mass hopper template," *Auton. Robots*, vol. 30, pp. 217–231, 2011.
- [20] M. H. Raibert, *Legged Robots that Balance*. Cambridge, MA, USA: MIT Press, 2000.
- [21] M. H. Raibert, "Trotting, pacing and bounding by a quadruped robot," *J. Biomechanics*, vol. 23, pp. 79–98, 1990.
- [22] T. Tanaka and S. Hirose, "Development of leg-wheel hybrid quadruped "AirHopper" design of powerful light-weight leg with wheel," in *Proc. IEEE/RSJ Int. Conf. Intell. Robots Syst.*, 2008, pp. 3890–3895.
- [23] J. A. Smith, I. Sharf, and M. Trentini, "Bounding gait in a hybrid wheeled-leg robot," in *Proc. IEEE/RSJ Int. Conf. Int. Robots Syst.*, 2006, pp. 5750–5755.
- [24] S. Bhattacharya, S. Chitta, V. Kumar, and D. Lee, "Optimization of a planar quadruped dynamic leap," in *Proc. ASME Int. Des. Eng. Tech. Conf. Comput. Inf. Eng. Conf.*, 2008, pp. 1101–1110.
- [25] M. Zucker, N. Ratliff, M. Stolle, J. Chestnutt, J. A. Bagnell, C. G. Atkeson, and J. Kuffner, "Optimization and learning for rough terrain legged locomotion," *Int. J. Robot. Res.*, vol. 30, pp. 175–191, Feb. 2011.
- [26] C. Zhu and A. Kawamura, "Development of biped robot MARI-3 for jumping," *Adv. Robot.*, vol. 24, pp. 1661–1675, 2010.
- [27] U. Saranlı, M. Buehler, and D. E. Koditschek, "RHex: A simple and highly mobile hexapod robot," *Int. J. Robot. Res.*, vol. 20, pp. 616–631, Jul. 2001.
- [28] P. C. Lin, H. Komsuoglu, and D. E. Koditschek, "Sensor data fusion for body state estimation in a hexapod robot with dynamical gaits," *IEEE Trans. Robot.*, vol. 22, no. 5, pp. 932–943, Oct. 2006.
- [29] D. McMordie and M. Buehler, "Towards pronking with a hexapod robot," in *Proc. Int. Conf. Climbing Walking Robots*, 2001.
- [30] A. M. Johnson, "Gait design using self-manipulation," in *Proc. Robot.: Sci. Syst.*, 2014.
- [31] A. M. Johnson and D. E. Koditschek, "Toward a vocabulary of legged leaping," in *Proc. IEEE Int. Conf. Robot. Autom.*, 2013, pp. 2553–2560.

- [32] BostonDynamics. *BigDog—The Most Advanced Rough-Terrain Robot on Earth*, 2014. [Online]. Available: http://www.bostondynamics.com/robot_bigdog.html
- [33] R. M. Alexander, *Elastic Mechanisms in Animal Movement*. Cambridge, U.K.: Cambridge Univ. Press 1988.
- [34] R. Blickhan, “The spring mass model for running and hopping,” *J. Biomechanics*, vol. 22, pp. 1217–1227, 1989.
- [35] C. T. Farley, J. Glasheen, and T. A. McMahon, “Running springs—Speed and animal size,” *J. Exp. Biol.*, vol. 185, pp. 71–86, Dec. 1993.
- [36] R. J. Full and D. E. Koditschek, “Templates and anchors: Neuromechanical hypotheses of legged locomotion on land,” *J. Exp. Biol.*, vol. 202, pp. 3325–3332, Dec. 1999.
- [37] J. Y. Jun and J. E. Clark, “Effect of rolling on running performance,” in *Proc. IEEE Int. Conf. Robot. Autom.*, 2011, pp. 2009–2014.
- [38] M. M. Ankaralı, E. Saygıner, Y. Yazıcıoğlu, A. Saranlı, and U. Saranlı, “A dynamic model of running with a half-circular compliant leg,” in *Proc. Int. Conf. Climbing Walking Robots*, 2012.
- [39] J. E. Seipel and P. Holmes, “A simple model for clock-actuated legged locomotion,” *Reg. Chaotic Dyn.*, vol. 12, pp. 502–520, Oct. 2007.
- [40] Y. C. Chou, W. S. Yu, K. J. Huang, and P. C. Lin, “Bio-inspired step-climbing in a hexapod robot,” *Bioinspiration Biomimetics*, vol. 7, p. 036008, Sep. 2012.
- [41] P. C. Lin, H. Komsuoğlu, and D. E. Koditschek, “A leg configuration measurement system for full-body pose estimates in a hexapod robot,” *IEEE Trans. Robot.*, vol. 21, no. 3, pp. 411–422, Aug. 2005.
- [42] K. J. Huang, C. K. Huang, and P. C. Lin, “A simple running model with rolling contact and its role as a template for dynamic locomotion on a hexapod robot,” *Bioinspiration Biomimetics*, vol. 9, p. 046004, 2014.
- [43] S. C. Chen, K. J. Huang, W. H. Chen, S. Y. Shen, C. H. Li, and P. C. Lin, “Quattroped: A leg-wheel transformable robot,” *IEEE/ASME Trans. Mechatronics*, vol. 19, no. 2, pp. 730–742, Apr. 2014.
- [44] W. H. Chen, H. S. Lin, and P. C. Lin, “TurboQuad: A leg-wheel transformable robot using bio-inspired control,” in *Proc. IEEE Int. Conf. Robot. Autom.*, 2014, p. 2090.
- [45] E. Z. Moore, D. Campbell, F. Grimmering, and M. Buehler, “Reliable stair climbing in the simple hexapod ‘RHex,’” in *Proc. IEEE Int. Conf. Robot. Autom.*, 2002, pp. 2222–2227.
- [46] D. Campbell and M. Buehler, “Stair descent in the simple hexapod ‘RHex,’” in *Proc. IEEE Int. Conf. Robot. Autom.*, 2003, vol. 1, pp. 1380–1385.



Ya-Cheng Chou received the B.S. and M.S. degrees in mechanical engineering from National Taiwan University, Taipei, Taiwan, in 2010 and 2012, respectively.

He is a Process Engineer with GARMIN Corporation, New Taipei, Taiwan. His research interests include robot dynamic and control, mechanism design, and bioinspired robotics.



Ke-Jung Huang received the B.S. and M.S. degrees in mechanical engineering from National Taiwan University, Taipei, Taiwan, in 2010 and 2012, respectively.

He is a Servo Control Engineer with Pegatron Corporation, Taipei. His research interests include computer programming, modeling, robot dynamics, and control.



Wei-Shun Yu received the B.S. and M.S. degrees in mechanical engineering from National Taiwan University, Taipei, Taiwan, in 2010 and 2012, respectively.

He was a Research Assistant with the Department of Mechanical Engineering, National Taiwan University, from 2013 to 2014. He is currently a Firmware Engineer with Kinpo Electronics Inc., Taipei, Taiwan. His research interests include computer programming, robot mechatronics design, and sensor applications.



Pei-Chun Lin (S'02–M'05) received the B.S. and M.S. degrees in mechanical engineering from National Taiwan University (NTU), Taipei, Taiwan, in 1996 and 1998, respectively, and the M.S. degree in electrical engineering and computer science and the Ph.D. degree in mechanical engineering from University of Michigan, Ann Arbor, MI, USA, in 2005.

He was a Postdoctoral Research Fellow with the Department of Materials Science and Engineering, University of Pennsylvania, Philadelphia, PA, USA, from 2005 to 2007. He is currently an Associate Professor with the Department of Mechanical Engineering, NTU. His research interests include bioinspired robotics, mechanical design, sensor design/fusion, control, dynamic locomotion, and compliant composites.

He is currently an Associate Professor with the Department of Mechanical Engineering, NTU. His research interests include bioinspired robotics, mechanical design, sensor design/fusion, control, dynamic locomotion, and compliant composites.